Geophysical Research Letters

RESEARCH LETTER
10.1029/2019GL083479

Contrasting Response of Precipitation to Aerosol Perturbation in the Tropics and Extratropics Explained by Energy Budget Considerations

Guy Dagan[1], **Philip Stier**[1], **and Duncan Watson-Parris**[1]

[1]Atmospheric, Oceanic and Planetary Physics, Department of Physics, University of Oxford, Oxford, UK

Key Points:
- Aerosol effect on precipitation is examined in terms of energetic constraints
- Aerosol perturbation generally increases precipitation in the tropics and decreases precipitation in the extratropics
- This behavior can be explained by contrasting ability of the atmosphere to diverge excess dry static energy in the two different regions

Supporting Information:
- Supporting Information S1

Correspondence to:
G. Dagan,
guy.dagan@physics.ox.ac.uk

Citation:
Dagan, G., Stier, P., & Watson-Parris, D. (2019). Contrasting response of precipitation to aerosol perturbation in the tropics and extratropics explained by energy budget considerations. *Geophysical Research Letters*, *46*, 7828–7837. https://doi.org/10.1029/2019GL083479

Received 29 APR 2019
Accepted 22 JUN 2019
Accepted article online 2 JUL 2019
Published online 10 JUL 2019

Abstract Precipitation plays a crucial role in the Earth's energy balance, the water cycle, and the global atmospheric circulation. Aerosols, by direct interaction with radiation and by serving as cloud condensation nuclei, may affect clouds and rain formation. This effect can be examined in terms of energetic constraints, that is, any aerosol-driven diabatic heating/cooling of the atmosphere will have to be balanced by changes in precipitation, radiative fluxes, or divergence of dry static energy. Using an aqua-planet general circulation model (GCM), we show that tropical and extratropical precipitation have contrasting responses to aerosol perturbations. This behavior can be explained by contrasting ability of the atmosphere to diverge excess dry static energy in the two different regions. It is shown that atmospheric heating in the tropics leads to large-scale thermally driven circulation and a large increase in precipitation, while the excess energy from heating in the extratropics is constrained due to the effect of the Coriolis force, causing the precipitation to decrease.

Plain Language Summary Precipitation, as the Earth's only natural source of fresh water, is of great importance for society. Climate change, besides changing the mean surface temperature and its distribution, is expected to change the precipitation's temporal and spatial distribution and, to a lesser extent, the global mean precipitation. One important agent in precipitation changes is anthropogenic aerosols. In this paper we study the response of precipitation to aerosol perturbations at different latitudes. Previously, it was proposed that aerosols drive a slowdown of the hydrological cycle. In addition, it was shown that, due to energy budget conservation, absorbing aerosols leads to a reduction in the global mean precipitation. Here we show that the response in the tropics is the opposite of the global mean response and of the extratropical response. Specifically, we show that the same aerosol perturbation generally increases precipitation in the tropics and decreases precipitation in the extratropics. This behavior can be explained by the contrasting ability of the atmosphere to diverge excess dry static energy in the tropics and extratropics. We also show that local aerosol perturbations could affect precipitation in remote regions due to a formation of large-scale circulation.

1. Introduction

Knowledge about cloud properties and rain formation is critical for understanding the current climate and for future climate predictions. Aerosols may influence cloud and rain properties by directly interacting with radiation and by acting as cloud condensation and ice nuclei (Altaratz et al., 2014; Levin & Cotton, 2009). The potential of aerosols to affect the climate system by changing the radiation balance and water cycle is well appreciated but far from being fully understood. Currently, most of the uncertainty in estimations of anthropogenic radiative forcing is attributed to radiation-aerosol and cloud-aerosol interactions (Boucher et al., 2013).

Aerosols may affect precipitation through a range of different pathways, which can be broadly grouped in the following categories:

1. By changing the microphysical properties of the clouds. This pathway has been shown to affect small spatial and temporal scales (e.g., Dagan et al., 2017; Fan et al., 2007; Jiang et al., 2006; Levin & Cotton, 2009, among many others). However, its effect on the larger and longer scales is not clear, and previous literature presents conflicting evidence (Dagan et al., 2018; Seifert et al., 2015; Stevens & Feingold, 2009).
2. By affecting the energy budget of the atmosphere. On long time scales, any aerosol-driven perturbation to the energy budget will have to be balanced by changes in precipitation, sensible heat flux, or by the

divergence of dry static energy (Fläschner et al., 2018; Hodnebrog et al., 2016; Mitchell et al., 1987; Muller & O'Gorman, 2011; Myhre et al., 2017; O'Gorman et al., 2012; Samset et al., 2016). Any change in precipitation via the microphysical pathway (Pathway 1) would also modify the atmospheric energy budget; hence, the two pathways are connected.

The second pathway, via the energy budget, is the focus of this study. On long time scales (neglecting the energy storage term), the atmospheric column energy budget is given by a balance between the enthalpy of vaporization (usually referred to as the latent heating rate, LP: the latent heat of condensation [L] multiplied by the surface precipitation rate [P]), the surface sensible heat flux (sometimes referred to as the sensible enthalpy flux [Q_{SH}]), the atmospheric radiative heating (Q_R, which is usually negative, representing cooling), and the divergence of dry static energy (div(s), which will become negligible on large spatial scales):

$$L\,P + Q_R + Q_{SH} = \mathrm{div}(s). \tag{1}$$

Q_R is the rate of net atmospheric diabatic heating due to radiative shortwave (SW) and longwave (LW) fluxes (F). It can be expressed by the sum of the surface (SFC) and top of the atmosphere (TOA) fluxes as follows:

$$Q_R = \left(F_{SW}^{TOA} - F_{SW}^{SFC}\right) - \left(F_{LW}^{TOA} - F_{LW}^{SFC}\right). \tag{2}$$

As in Naegele and Randall (2019), in (2), LW fluxes are positive upward, and SW fluxes are positive downward.

Recently, it was shown that the temporal changes in the tropical (extratropical) precipitation rate are positively (negatively) correlated with temporal changes in Q_R (Naegele & Randall, 2019). This trend was explained by different feedbacks of clouds on Q_R in the two different regimes. According to (1), positive correlation between LP and Q_R must mean a significant change in Q_{SH} (which is expected to be bounded) or in the divergent term. This might suggest that there is another fundamental difference between the tropics and the extratropics that can explain the difference in the correlation between Q_R and LP—the differences in the Rossby radius of deformation (Rd; Charney, 1963). In the tropics, due to small Coriolis effect, Rd is very large, and hence, horizontal temperature (or dry static energy) gradients are weak (Sobel et al., 2001). Consequently, any aerosol (or other) perturbation to the Q_R could be distributed on large spatial scales through the mechanism of equatorial internal waves (Gill, 1980; Matsuno, 1966). In addition, aerosol warming (absorption) can lead to thermally direct circulations and associated moisture convergence (Roeckner et al., 2006), which could also distribute the Q_R perturbation on large scales. A similar mechanism may be operating on the aerosol effect on monsoon dynamics and precipitation (Bollasina et al., 2011; Hodnebrog et al., 2016; Menon et al., 2002; Roeckner et al., 2006). In the extratropics on the other hand, the relatively small Rd (~1,000 km) implies that no large-scale thermally direct circulations can be formed by diabatic heating, and hence, the divergence of dry static energy is expected to be confined to smaller scales. The abovementioned difference between the tropics and extratropics can also be put in terms of the concept of "geostrophic adjustment" (Mihaljan, 1963; Rossby, 1938; Vallis, 2006), that is, in the extratropics, heating perturbations will be confined through geostrophic adjustment of the flow to the heating. In the tropics, on the other hand, the mass field adjusts to the heating, that is, mass converges into the heating anomaly, which then generate vertical motion and an increase in precipitation.

We note that the energetic constraints (equation (1)) hold only for the mean precipitation rate and not for the distribution of rainfall intensities, which could be modified even under energetic constraints on mean precipitation rate.

Perturbations to the Q_R due to aerosols at different geographical locations could also have different effects on the general circulation of the atmosphere (Chemke & Dagan, 2018). For example, interhemispheric asymmetry in Q_R may lead to a shift in the intertropical convergence zone due to cross equatorial energy flux (Allen et al., 2015; Ming & Ramaswamy, 2011; Rotstayn & Lohmann, 2002; Voigt et al., 2017; Wang, 2015). Aerosols may also affect the atmospheric circulation in the extratropics by decreasing the meridional energy fluxes (Ming et al., 2011; Ming & Ramaswamy, 2011) and shifting the extratropical jets poleward (Allen & Sherwood, 2011; Chemke & Dagan, 2018). It was also shown, in idealized aqua-plant simulations that zonal gradients in aerosol radiative forcing may lead to an equatorial superrotating jet due to

convergence of eddy-momentum fluxes (Chemke & Dagan, 2018). Similar behavior was shown in simulations of tidally locked exoplanets (Merlis & Schneider, 2010).

In this study we use an aqua-planet GCM to study the fast precipitation response (i.e., under prescribed sea surface temperatures [SSTs]; Bony et al., 2013; Richardson et al., 2018) to net diabatic heating due to aerosols in the tropics and extratropics. Previously, it was proposed that an increase in aerosols may lead to a slowdown of the hydrological cycle (Ramanathan et al., 2001), and specifically, it was shown that an increase in absorbing aerosols leads to a reduction of the global mean precipitation (e.g., Samset et al., 2016). Here we examine the response at different latitudes.

2. Methodology

The icosahedral non hydrostatic (ICON) atmospheric general circulation model (Crueger et al., 2018; Giorgetta et al., 2018; Zängl et al., 2015) is used in an aqua-planet configuration using prescribed SST. Altogether, 17 simulations are conducted—one reference simulation with no aerosol forcing and 16 simulations with different aerosol plume characteristics. The reference simulation is run for 10 years to achieve low noise and zonally symmetric conditions (see Figure S1 in the supporting information), while each of the perturbed simulations is run for 4 years, which is sufficient to reach a stationary state. Seasonal variations are not considered. The simulations are conducted with 47 vertical levels. The ICON grid R2B04 is used, which has an effective resolution of 157.8 km (Zängl et al., 2015).

3. Representation of the Aerosol Effect

For representing the radiative effect of aerosols, the Max Planck Institute Aerosol Climatology version 2, Simple Plume (MACv2-SP; Kinne et al., 2013; Stevens et al., 2017) parametrization is used. MACv2-SP was designed to represent, in a simple and efficient way, the spatiotemporal distributions of anthropogenic aerosol's optical properties. It represents both the direct aerosol effect and the Twomey effect (i.e., increase in cloud albedo due to an increase in droplet concentration under constant liquid water path; Twomey, 1977). No other cloud-aerosol effects, such as changes in liquid water path (Albrecht, 1989), are considered. MACv2-SP prescribes the anthropogenic aerosol optical depth (AOD) and its radiative properties, including the asymmetry parameter and the single scattering albedo (SSA), as functions of geographical location, time, and wavelength. In our case, we remove both the seasonal and interannual variations and use idealized constant aerosol conditions for each simulation. MACv2-SP represents the spatial distribution of each plume by two features: a rotated Gaussian feature, which represents the AOD in the vicinity of the source, and a piecewise Gaussian feature, which represents the aerosols' transport and asymmetric distributions of sources and sinks (Stevens et al., 2017). In our case, for simplicity, only the former is used, and no rotation is applied; hence, the spatial distribution around the plume center is a simple Gaussian distribution. The radius of the plume is varied between 5°, 10°, 15°, and 25° in both the north-south and east-west directions. To investigate the effects of aerosols on precipitation in different geographical locations, we use two different aerosol plume locations: in the tropics (centered at 0°N, 0°W) and in the northern hemisphere extratropics (centered at 40°N, 0°W). The magnitude of the AOD at the center of the tropical plume is equal to the global sum of all plumes in the default MACv2-SP setup (AOD at the center of the plume = 2.4). For comparison between the tropics and extratropics (for each plume size), corrections for the differing amounts of incoming solar radiation and for the different width of a degree longitude are applied by increasing the AOD magnitude at the center of the plume and the plume zonal dimensions by a factor of $1/\cos(40°)$. Hence, for each plume size, the global mean radiative forcing is similar between the tropical and extratropical simulations. The vertical distribution of aerosol is based on the kernel of Euler's β function (see details in Stevens et al., 2017) and is mostly confined to below 5 km. Differences in the vertical placement of the plume may cause different response of the climate system and general circulation (Ban-Weiss et al., 2012; Kim et al., 2015); however, they are less important to the column-integrated energy budget, which is the focus of this study. For each plume size and location, two different cases of SSA (representing the radiative properties of the aerosols) are simulated—0.8 (representing relatively absorbing plumes) and 0.95 (representing less absorbing plumes). The Q_R result for each simulation is presented in Figure S2.

In this study we focus on the fast precipitation response (Bony et al., 2013; Richardson et al., 2018). We note that concentrating the AOD's global sum over a small region (as was done in this study) results in a large

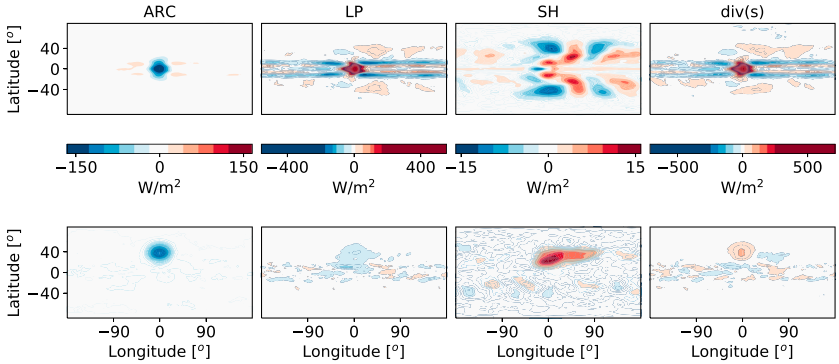

Figure 1. Changes of atmospheric energy budget terms (Q_R = atmospheric radiative heating, first column; *LP* - enthalpy of vaporization due to precipitation, second column; Q_{SH} = sensible heat flux, third column; and div(*s*) = divergence of dry static-energy, fourth column) in response to introduction of idealized aerosol plumes with the same plume size (10°) and the same aerosol optical properties (single scattering albedo = 0.8) but different plume location, at the tropics (upper row) and extratropics (lower row). Note the different color bars for the different terms.

local aerosol-driven changes in Q_R. This helps in detecting the aerosol effect and the different mechanisms operating in the tropics and extratropics.

4. Results

Examining the global mean properties demonstrates that, as expected, the global mean precipitation rate is linearly affected by the changes in the Q_R (Figure S3). Generally, the larger the plume and the more absorbing it is (SAA of 0.8 compared to 0.95), the larger the change in Q_R and hence also in *LP* (e.g., slowdown of the hydrological cycle; Ramanathan et al., 2001), regardless of the plume location. Focusing on the fast precipitation response, using prescribed SSTs, the main effect of the aerosol plumes is to heat the atmosphere by absorption (stronger effect for SAA of 0.8 compared to 0.95).

To set the stage, we examine the differences from the reference simulation (Figure S1) of the terms in equation (1) under two simulations with the same plume size (10°) and the same aerosol optical properties (SSA = 0.8), that is, with the same global mean perturbation but different plume location in the tropics (hereafter "tropical" simulation) and extratropics (hereafter "extratropical" simulation, Figure 1). The two simulations produce a similar magnitude and spatial extent of Q_R driven by a similar aerosol radiative forcing. Small differences do appear in Q_R between the two simulations with the tropical Q_R being slightly higher (by 24% at the plume center) due to cloud feedbacks (see section S1 and Figures S4 and S5). However, the similarly forced Q_R produces remarkably different local precipitation responses: The local precipitation increases significantly in the tropical simulation, while in the extratropical simulation, it slightly decreases. We note that the local response in the tropical simulation of an increase in precipitation is the opposite to the global mean response of decrease in precipitation (Figure S3). In the tropical simulation, the precipitation is reduced along most of the double intertropical convergence zone band (see Figure S1) and increases in the extratropics, east of the plume center. The Q_{SH} flux changes are an order of magnitude smaller than the Q_R and precipitation changes and show a local decrease in the extratropical simulation. In the tropical simulation, the Q_{SH} flux increases downwind and decreases upwind of the center of the plume. Also, in the tropical simulation, the Q_{SH} flux changes in the extratropics in both hemispheres, and its structure suggests a resulting standing wave (see also Figure 3). This structure demonstrates that aerosol perturbations could have implications for precipitation in remote regions and suggests that some wave-teleconnections mechanism is operating in response to local perturbations. The divergence of dry static energy is calculated as the residual of all other terms. It shows a large increase in the tropical simulation (about 4.3 times larger than the change in the Q_R), spatially matching the *LP* change pattern, and only a small increase in the extratropical simulation (about 63% of the Q_R change).

Examining the local (plume center) response of all the different simulations (Figure 2) demonstrates a similar trend. For all plume sizes and SSAs, a similar aerosol plume results in a slightly higher Q_R in the tropics

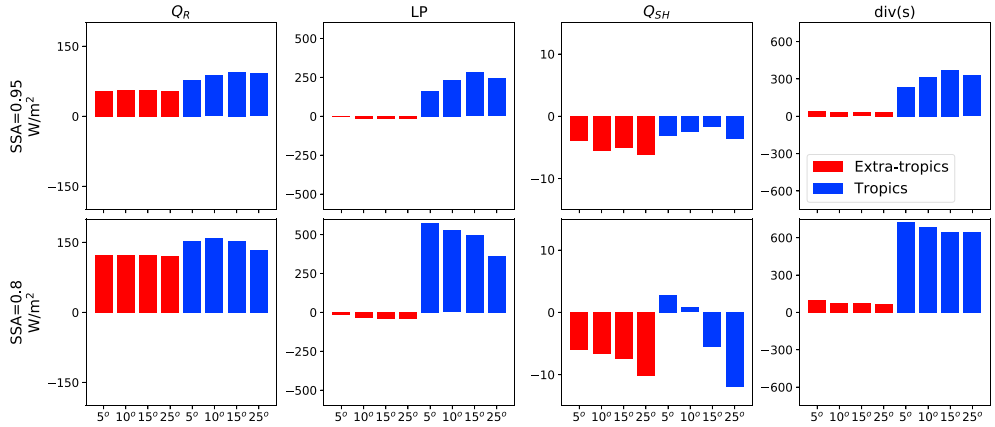

Figure 2. Changes in atmospheric energy budget terms (Q_R = atmospheric radiative heating, *LP* - enthalpy of vaporization due to precipitation, Q_{SH} = sensible heat flux, and div(*s*) = divergence of dry static-energy) at the center of the aerosol plume for each of the perturbed simulations (presented as differences from the reference simulation). Blue bars represent aerosol plumes centered at the tropics (0°N, 0°W), while red bars represent aerosol plumes centered at the extratropics (40°N, 0°W). The upper and lower rows are for SSA = 0.95 and SSA = 0.8, respectively. The different bars at each panel represent the different plume sizes. SSA = single scattering albedo.

compared with the extratropics (by 27% on average) due to cloud feedbacks (see section S1 and Figures S4 and S5). Interestingly, comparable Q_R drives a large increase in precipitation in the tropics (*LP* is a factor of 2.9 larger than the Q_R magnitude on average) but a decrease in the extratropics (of about 0.25 of the Q_R magnitude on average). This trend cannot be explained by the relatively small changes in the Q_{SH} flux which is only marginally larger (in magnitude) in the extratropics than in the tropics (for a given plume size and SSA). In addition, for all aerosol plume conditions, the tropical simulations produce a very large increase in the divergence of dry static energy (by a factor of 3.9 larger than the Q_R on average), with only a small change in the extratropics (of about two thirds of the Q_R on average).

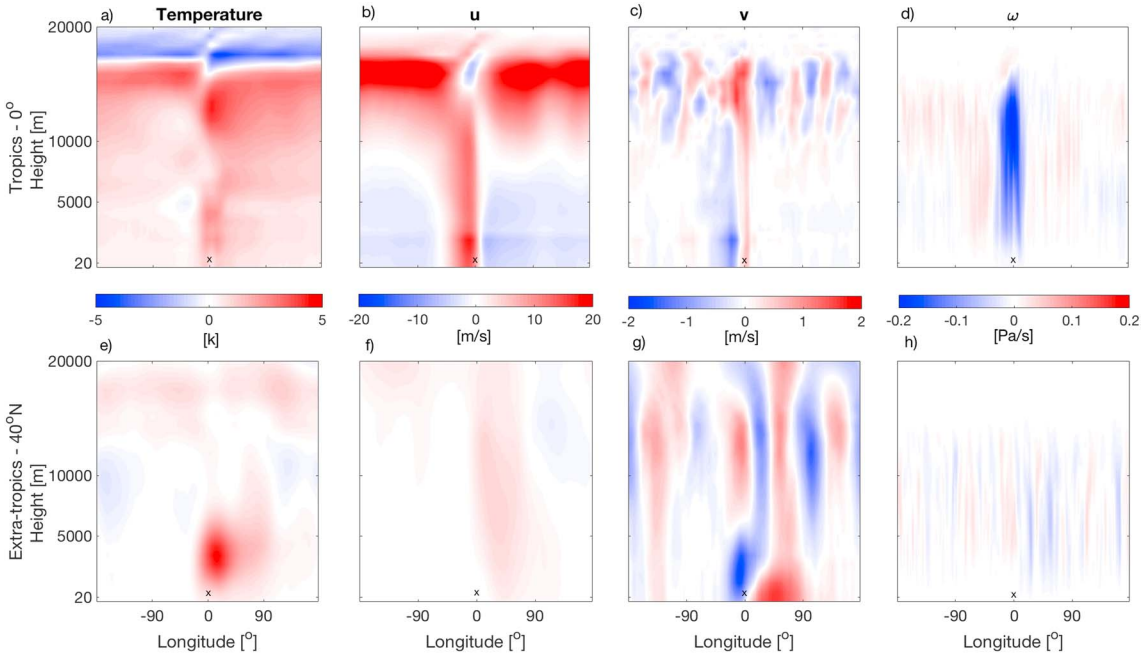

Figure 3. Zonal cross sections across the latitude of the aerosol plumes' center (marked by "x") of differences from the reference simulation in temperature (a and e), eastward winds, *u* (b and f), northward winds, *v* (c and g), and vertical winds, ω (d and h). The upper row (a–d) presents the tropical simulation (cross section across latitude 0°), while the lower row (e–h) presents the extratropical simulation (cross section across latitude 40°N). These two simulations are the same as in Figure 1.

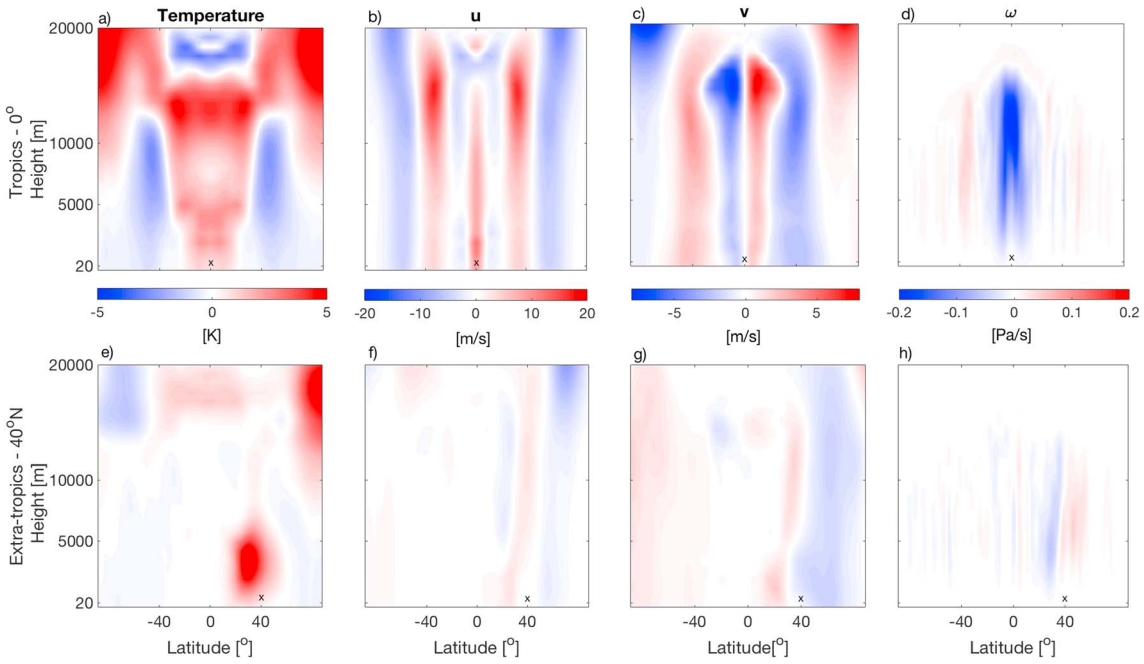

Figure 4. Meridional cross sections across the longitude of the aerosol plumes' center (longitude 0°; marked by "x") of differences from the reference simulation in temperature (a and e), eastward winds, *u* (b and f), northward winds, *v* (c and g), and vertical winds, ω (d and h). The upper row (a–d) presents the tropical simulation, while the lower row (e–h) presents the extratropical simulation. These two simulations are the same as in Figure 1.

We also note that, for the same AOD, the more absorbing aerosol plumes (SSA = 0.8) result in stronger response than the less absorbing aerosol plumes (SSA = 0.95), since under fixed SSTs, the main change to the atmospheric energy budget is due to atmospheric absorption. In addition, in the case of the strongest precipitation response (tropical plume with SSA = 0.8), increasing the plume size results in a reduction of the precipitation response at the plume's center.

In order to explain the contrasting response of precipitation to aerosol forcing in the tropics and extratropics, we examine the response of the atmospheric dynamics and thermodynamics. Figures 3 and 4 present the differences from the reference simulations of the zonal and meridional vertical cross section across the aerosol plumes' center, respectively, for the simulations presented in Figure 1. The zonal cross sections demonstrate that the aerosol perturbation in the extratropical simulation produces warming in the lower atmosphere (below 5 km—the altitude in which the aerosols are mainly located) which is also confined in its horizontal extent (Figure 3e). It also demonstrates that the warming in the extratropical simulation is tilted to the east of the plume center, as a result of the dominating eastward winds in the extratropics that advect the signal. However, in the tropical simulation, most of the warming is confined to the upper troposphere (9–12 km) at all longitudes (Figure 3a). In the tropical simulation, there is also a cooling of the stratosphere which is consistent with the decrease in the outgoing LW flux (Figure S4; Ramanathan, 1988). The eastward wind (*u*) changes demonstrate almost no effect of the aerosol perturbation in the extratropical simulation and a very significant effect in the tropical simulation (Figures 3b and 3f). In the tropical simulation, the lower atmosphere has an increase in *u* west of the plume's center (longitude 0°) and a slight decrease of *u* east of it, which implies convergence at the plume's center. In the upper troposphere, there is a large increase in *u,* indicating the existence of an equatorial superrotating jet. Previously, it was shown that zonally asymmetric diabatic heating can lead to convergence of eddy-momentum fluxes at the equator and superrotating jet (Chemke & Dagan, 2018; Merlis & Schneider, 2010). The changes in the northward winds (*v*; Figures 3c and 3g) show an increase and a decrease side by side in both simulations (but the changes are generally stronger in the extratropical simulation). This behavior indicates that standing waves are formed around the aerosol plume due to the local heating (e.g., Kaspi & Schneider, 2011). The changes in the vertical velocity (*ω*) are consistent with the changes in the temperature and *u* and demonstrate an increased upward motion. This is indicative of a thermally direct circulation at the plume's location in the tropical simulation and a negligible change in the extratropical simulation.

The meridional cross sections of changes in temperature across the plumes' centers indicate again that the aerosol perturbation is well confined in both the vertical and horizontal directions in the extratropical simulation (Figure 4e). Here, again, the temperature change is not perfectly colocated with the aerosol plume due to advection (see the negative v perturbation north of the plume center; Figure 4g) and asymmetric incoming solar radiation (compared to the plume center). In the tropical simulation, on the other hand, the temperature perturbation is distributed throughout the entire tropical region and is more pronounced in the upper troposphere (Figure 4a). The horizontal extent of the temperature change in the tropical simulation can be understood by the weak temperature gradient arguments (Sobel et al., 2001), while the amplification of the warming in the upper troposphere is expected due to changes in the moist adiabatic lapse rate (Held & Soden, 2006; O'Gorman & Singh, 2013). All three wind components exhibit a weak response to the aerosol plume in the extratropical simulation (Figures 4f–4h) and a large response in the tropical simulation (Figures 4b–4d). In the tropical simulation, the jet strength in both hemispheres increases, shown by an increase in u, which is caused by the increase in the equator-to-pole temperature difference (Figure 4a; as predicted by thermal wind balance). This occurs concomitantly with an increase in the northward and southward winds in the upper northern and southern parts of the Hadley cell, respectively, and an increase in the upward motion of air at the equator. These all point to a local increase in the Hadley circulation strength around the plume.

5. Summary

Our analysis (Figures 1 and 2) demonstrates a remarkably different local response of precipitation to aerosol-driven perturbations in Q_R in the tropics and extratropics. While the diabatic heating in the tropics leads to a large local increase in precipitation (amplified by almost a factor of 3 compared to the forced Q_R in terms of energy flux units; Figure 2), in the extratropics, the precipitation decreases. The increase in the local precipitation in the tropics occurs despite a decrease in the global mean precipitation, while the local decrease in precipitation in the extratropics has a similar sign to the global mean response and is more intuitive from the energy budget perspective.

We have shown that in the tropics, the induced warming leads to both thermally driven zonal circulation (Figure 3; Roeckner et al., 2006) and intensification of the meridional circulation (the Hadley circulation; Figure 4). These large-scale circulations diverge the excess dry static energy very efficiently (Figures 1 and 2) and distribute the warming throughout the entire tropical region (Figures 3 and 4). In addition to the local strong increase in precipitation in the tropical simulation, the precipitation in other regions (both in the tropics and in the extratropics) is modified as well. This suggests a potential mechanism for teleconnections in response to aerosol perturbations, which could have implication on precipitation at different regions. Contrastingly, in the extratropics, the induced warming stays confined to the plume's location, and no large-scale circulation is formed. This can be attributed to the larger effect of Coriolis force in the extratropics than in the tropics. The absence of an induced large-scale circulation in the extratropics and the relatively small Rossby radius of deformation (Charney, 1963) results in a low divergence of dry static energy (Figures 1 and 2). Thus, the small effect of the divergence implies that net atmospheric diabatic heating (e.g., by absorbing aerosols) would have to be balanced by decrease in the enthalpy of vaporization due to precipitation. Another way to understand this trend is via the concept of geostrophic adjustment. In agreement with theory (Vallis, 2006), we show that heating anomalies in the extratropics are constrained through geostrophic adjustment, which is to say that the winds adjust to and balance the destabilization caused by the heating. In the tropics, on the other hand, mass is converged into the heating anomaly to balance it. Since near-surface convergence is strongly related to precipitation, the mass response in the tropics is associated with a positive precipitation anomaly. The same trend in the extratropics was found in a multimodel, more "realistic," fast response simulations as a response to black carbon emissions (Samset et al., 2016). The mechanism proposed here, based on idealized simulations, can explain this trend.

Another interesting result shown by these simulations is that in the case of the strongest response in precipitation (tropical plume with SSA = 0.8), increasing the plume size drives a reduction of the response of the precipitation at the plume's center (Figure 2). We speculate that this is because the atmosphere's ability to diverge dry static energy decreases with the spatial scale of the perturbation. This should be further

investigated in future work. In addition, the differences between the tropics and extratropic in the slow precipitation response (due to changes in SST) are still to be determined.

As was hypothesized in Naegele and Randall (2019), the difference between the tropics and extratropics may have implications to convective self-aggregation. Our tropical simulations generated convective *forced* aggregation (as opposed to self-aggregation); however, some similarities do exist. Convective aggregation involves large-scale circulations driven by increase in enthalpy of vaporization in the aggregated clouds and horizontal gradients of Q_R (Bretherton et al., 2005). The efficiency of the tropical atmosphere to diverge dry static energy, and hence generate such a circulation, may promote convective aggregations which might have implication for cloud feedback to global warming (Bony et al., 2015; Bretherton & Khairoutdinov, 2015; Vogel et al., 2016).

In summary, our results show a contrasting response of precipitation to absorbing aerosol between the tropics and the extratropics, where absorbing aerosol generally increases precipitation in the tropics and decreases precipitation in the extratropics. Previously, it was proposed that aerosols drive a slowdown of the hydrological cycle (Ramanathan et al., 2001) and that the presence of absorbing aerosols leads to a reduction of the global mean precipitation (e.g., Samset et al., 2016), as expected by the energy budget constraint. Here we show that the local response in the tropics is the opposite of the global mean response expected from energetic considerations.

Acknowledgments
This research was supported by the European Research Council (ERC) project constRaining the EffeCts of Aerosols on Precipitation (RECAP) under the European Union's Horizon 2020 research and innovation programme with grant agreement 724602. P. S. also acknowledges support by the Alexander von Humboldt Foundation. D. W. P. and P. S. additionally acknowledge funding from Natural Environment Research Council projects NE/L01355X/1 (CLARIFY) and NE/P013406/1 (A-CURE). The simulations were performed using the ARCHER UK National Supercomputing Service. We thank Raymond Pierrehumbert for very fruitful discussions during the preparation of this paper. All the data used in this publication can be found online (https://doi.org/10.5281/zenodo.3242319).

References

Albrecht, B. A. (1989). Aerosols, cloud microphysics, and fractional cloudiness. *Science (New York, NY)*, *245*(4923), 1227–1230. https://doi.org/10.1126/science.245.4923.1227

Allen, R. J., Evan, A. T., & Booth, B. B. (2015). Interhemispheric aerosol radiative forcing and tropical precipitation shifts during the late twentieth century. *Journal of Climate*, *28*(20), 8219–8246. https://doi.org/10.1175/JCLI-D-15-0148.1

Allen, R. J., & Sherwood, S. C. (2011). The impact of natural versus anthropogenic aerosols on atmospheric circulation in the Community Atmosphere Model. *Climate Dynamics*, *36*(9-10), 1959–1978. https://doi.org/10.1007/s00382-010-0898-8

Altaratz, O., Koren, I., Remer, L., & Hirsch, E. (2014). Review: Cloud invigoration by aerosols—Coupling between microphysics and dynamics. *Atmospheric Research*, *140-141*, 38–60. https://doi.org/10.1016/j.atmosres.2014.01.009

Ban-Weiss, G. A., Cao, L., Bala, G., & Caldeira, K. (2012). Dependence of climate forcing and response on the altitude of black carbon aerosols. *Climate Dynamics*, *38*(5-6), 897–911. https://doi.org/10.1007/s00382-011-1052-y

Bollasina, M. A., Ming, Y., & Ramaswamy, V. (2011). Anthropogenic aerosols and the weakening of the South Asian Summer Monsoon. *Science*, *334*(6055), 502–505. https://doi.org/10.1126/science.1204994

Bony, S., Bellon, G., Klocke, D., Sherwood, S., Fermepin, S., & Denvil, S. (2013). Robust direct effect of carbon dioxide on tropical circulation and regional precipitation. *Nature Geoscience*, *6*(6), 447–451. https://doi.org/10.1038/ngeo1799

Bony, S., Stevens, B., Frierson, D. M. W., Jakob, C., Kageyama, M., Pincus, R., et al. (2015). Clouds, circulation and climate sensitivity. *Nature Geoscience*, *8*(4), 261–268. https://doi.org/10.1038/ngeo2398

Boucher, O., Randall, D., Artaxo, P., Bretherton, C., Feingold, G., Forster, P., et al. (2013). Clouds and aerosols. In *Climate change 2013: the physicalscience basis. Contribution of Working Group I to the Fifth Assessment Report of the intergovernmental Panel on Climate Change*. Cambridge: Cambridge University Press (pp. 571–657).

Bretherton, C. S., Blossey, P. N., & Khairoutdinov, M. (2005). An energy-balance analysis of deep convective self-aggregation above uniform SST. *Journal of the Atmospheric Sciences*, *62*(12), 4273–4292. https://doi.org/10.1175/JAS3614.1

Bretherton, C. S., & Khairoutdinov, M. F. (2015). Convective self-aggregation feedbacks in near-global cloud-resolving simulations of an aquaplanet. *Journal of Advances in Modeling Earth Systems*, *7*, 1765–1787. https://doi.org/10.1002/2015MS000499

Charney, J. G. (1963). A note on large-scale motions in the tropics. *Journal of the Atmospheric Sciences*, *20*(6), 607–609. https://doi.org/10.1175/1520-0469(1963)020<0607:ANOLSM>2.0.CO;2

Chemke, R., & Dagan, G. (2018). The effects of the spatial distribution of direct anthropogenic aerosols radiative forcing on atmospheric circulation. *Journal of Climate*, *31*(17), 7129–7145. https://doi.org/10.1175/JCLI-D-17-0694.1

Crueger, T., Giorgetta, M. A., Brokopf, R., Esch, M., Fiedler, S., Hohenegger, C., et al. (2018). ICON-A: The atmospheric component of the ICON Earth System Model. Part II: Model evaluation. *Journal of Advances in Modeling Earth Systems*, *10*, 1638–1662. https://doi.org/10.1029/2017MS001233

Dagan, G., Koren, I., Altaratz, O., & Heiblum, R. H. (2017). Time-dependent, non-monotonic response of warm convective cloud fields to changes in aerosol loading. *Atmospheric Chemistry and Physics*, *17*(12), 7435–7444. http://www.atmos-chem-phys.net/17/7435/2017/, https://doi.org/10.5194/acp-17-7435-2017

Dagan, G., Koren, I., Altaratz, O., & Lehahn, Y. (2018). Shallow convective cloud field lifetime as a key factor for evaluating aerosol effects. *iScience*, *10*, 192–202. https://doi.org/10.1016/j.isci.2018.11.032

Fan, J., Zhang, R., Li, G., Tao, W.-K., & Li, X. (2007). Simulations of cumulus clouds using a spectral microphysics cloud-resolving model. *Journal of Geophysical Research*, *112*, D04201. https://doi.org/10.1029/2006JD007688

Fläschner, D., Mauritsen, T., Stevens, B., & Bony, S. (2018). The signature of shallow circulations, not cloud radiative effects, in the spatial distribution of tropical precipitation. *Journal of Climate*, *31*(23), 9489–9505. https://doi.org/10.1175/JCLI-D-18-0230.1

Gill, A. E. (1980). Some simple solutions for heat-induced tropical circulation. *Quarterly Journal of the Royal Meteorological Society*, *106*(449), 447–462. https://doi.org/10.1002/qj.49710644905

Giorgetta, M. A., Brokopf, R., Crueger, T., Esch, M., Fiedler, S., Helmert, J., et al. (2018). ICON-A, the atmosphere component of the ICON Earth System Model. Part I: Model description. *Journal of Advances in Modeling Earth Systems*, *10*, 1613–1637. https://doi.org/10.1029/2017MS001242

Held, I. M., & Soden, B. J. (2006). Robust responses of the hydrological cycle to global warming. *Journal of Climate*, *19*(21), 5686–5699. https://doi.org/10.1175/JCLI3990.1

Hodnebrog, O., Myhre, G., Forster, P. M., Sillmann, J., & Samset, B. H. (2016). Local biomass burning is a dominant cause of the observed precipitation reduction in southern Africa. *Nature Communications*, *7*(1). https://doi.org/10.1038/ncomms11236

Jiang, H., Xue, H., Teller, A., Feingold, G., & Levin, Z. (2006). Aerosol effects on the lifetime of shallow cumulus. *Geophysical Research Letters*, *33*, L14806. https://doi.org/10.1029/2006GL026024

Kaspi, Y., & Schneider, T. (2011). Winter cold of eastern continental boundaries induced by warm ocean waters. *Nature*, *471*(7340), 621–624. https://doi.org/10.1038/nature09924

Kim, H., Kang, S. M., Hwang, Y.-T., & Yang, Y.-M. (2015). Sensitivity of the climate response to the altitude of black carbon in the northern subtropics in an Aquaplanet GCM. *Journal of Climate*, *28*(16), 6351–6359. https://doi.org/10.1175/JCLI-D-15-0037.1

Kinne, S., O'Donnel, D., Stier, P., Kloster, S., Zhang, K., Schmidt, H., et al. (2013). MAC-v1: A new global aerosol climatology for climate studies. *Journal of Advances in Modeling Earth Systems*, *5*, 704–740. https://doi.org/10.1002/jame.20035

Levin, Z., & Cotton, W. R. (2009). In Z. Levin, & W. R. Cotton (Eds.), *Aerosol pollution impact on precipitation: A scientific review*. New York: Springer. https://doi.org/10.1007/978-1-4020-8690-8

Matsuno, T. (1966). Quasi-geostrophic motions in the equatorial area. *Journal of the Meteorological Society of Japan. Series II*, *44*(1), 25–43. https://doi.org/10.2151/jmsj1965.44.1_25

Menon, S., Hansen, J., Nazarenko, L., & Luo, Y. F. (2002). Climate effects of black carbon aerosols in China and India. *Science*, *297*(5590), 2250–2253. https://doi.org/10.1126/science.1075159

Merlis, T. M., & Schneider, T. (2010). Atmospheric dynamics of Earth-like tidally locked Aquaplanets. *Journal of Advances in Modeling Earth Systems*, *2*, 13. https://doi.org/10.3894/JAMES.2010.2.13

Mihaljan, J. M. (1963). The exact solution of the Rossby adjustment problem. *Tellus*, *15*(2), 150–154. https://doi.org/10.3402/tellusa.v15i2.8833

Ming, Y., & Ramaswamy, V. (2011). A model investigation of aerosol-induced changes in tropical circulation. *Journal of Climate*, *24*(19), 5125–5133. https://doi.org/10.1175/2011JCLI4108.1

Ming, Y., Ramaswamy, V., & Chen, G. (2011). A model investigation of aerosol-induced changes in boreal winter extratropical circulation. *Journal of Climate*, *24*(23), 6077–6091. https://doi.org/10.1175/2011JCLI4111.1

Mitchell, J., Wilson, C., & Cunnington, W. (1987). On CO_2 climate sensitivity and model dependence of results. *Quarterly Journal of the Royal Meteorological Society*, *113*(475), 293–322. https://doi.org/10.1256/smsqj.47516

Muller, C., & O'Gorman, P. (2011). An energetic perspective on the regional response of precipitation to climate change. *Nature Climate Change*, *1*(5), 266–271. https://doi.org/10.1038/nclimate1169

Myhre, G., Forster, P. M., Samset, B. H., Hodnebrog, Ø., Sillmann, J., Aalbergsjø, S. G., et al. (2017). PDRMIP: A precipitation driver and response model intercomparison project—Protocol and preliminary results. *Bulletin of the American Meteorological Society*, *98*(6), 1185–1198. https://doi.org/10.1175/BAMS-D-16-0019.1

Naegele, A., & Randall, D. (2019). Geographical and seasonal variability of cloud-radiative feedbacks on precipitation. *Journal of Geophysical Research: Atmospheres*, *124*, 684–699. https://doi.org/10.1029/2018JD029186

O'Gorman, P. A., Allan, R. P., Byrne, M. P., & Previdi, M. (2012). Energetic constraints on precipitation under climate change. *Surveys in Geophysics*, *33*(3-4), 585–608. https://doi.org/10.1007/s10712-011-9159-6

O'Gorman, P. A., & Singh, M. S. (2013). Vertical structure of warming consistent with an upward shift in the middle and upper troposphere. *Geophysical Research letters*, *40*, 1838–1842. https://doi.org/10.1002/grl.50328

Ramanathan, V. (1988). The greenhouse theory of climate change: A test by an inadvertent global experiment. *Science*, *240*(4850), 293–299. https://doi.org/10.1126/science.240.4850.293

Ramanathan, V., Crutzen, P., Kiehl, J., & Rosenfeld, D. (2001). Aerosols, climate, and the hydrological cycle. *Science*, *294*(5549), 2119–2124. https://doi.org/10.1126/science.1064034

Richardson, T. B., Forster, P. M., Andrews, T., Boucher, O., Faluvegi, G., Fläschner, D., et al. (2018). Drivers of precipitation change: An energetic understanding. *Journal of Climate*, *31*(23), 9641–9657. https://doi.org/10.1175/JCLI-D-17-0240.1

Roeckner, E., Stier, P., Feichter, J., Kloster, S., Esch, M., & Fischer-Bruns, I. (2006). Impact of carbonaceous aerosol emissions on regional climate change. *Climate Dynamics*, *27*(6), 553–571. https://doi.org/10.1007/s00382-006-0147-3

Rossby, C. G. (1938). On the mutual adjustment of pressure and velocity distribution in certain simple current systems, II. *Journal of Marine Research*, *1*(3), 239–263. https://doi.org/10.1357/002224038806440520

Rotstayn, L. D., & Lohmann, U. (2002). Tropical rainfall trends and the indirect aerosol effect. *Journal of Climate*, *15*(15), 2103–2116. https://doi.org/10.1175/1520-0442(2002)015<2103:TRTATI>2.0.CO;2

Samset, B. H., Myhre, G., Forster, P. M., Hodnebrog, Ø., Andrews, T., Faluvegi, G., et al. (2016). Fast and slow precipitation responses to individual climate forcers: A PDRMIP multimodel study. *Geophysical Research Letters*, *43*, 2782–2791. https://doi.org/10.1002/2016GL068064

Seifert, A., Heus, T., Pincus, R., & Stevens, B. (2015). Large-eddy simulation of the transient and near-equilibrium behavior of precipitating shallow convection. *Journal of Advances in Modeling Earth Systems*, *7*, 1918–1937. https://doi.org/10.1002/2015MS000489

Sobel, A. H., Nilsson, J., & Polvani, L. M. (2001). The weak temperature gradient approximation and balanced tropical moisture waves. *Journal of the Atmospheric Sciences*, *58*(23), 3650–3665. https://doi.org/10.1175/1520-0469(2001)058<3650:TWTGAA>2.0.CO;2

Stevens, B., & Feingold, G. (2009). Untangling aerosol effects on clouds and precipitation in a buffered system. *Nature*, *461*(7264), 607–613. https://doi.org/10.1038/nature08281

Stevens, B., Fiedler, S., Kinne, S., Peters, K., Rast, S., Müsse, J., et al. (2017). MACv2-SP: A parameterization of anthropogenic aerosol optical properties and an associated Twomey effect for use in CMIP6. *Geoscientific Model Development*, *10*(1), 433–452. https://doi.org/10.5194/gmd-10-433-2017

Twomey, S. (1977). The influence of pollution on the shortwave albedo of clouds. *Journal of the Atmospheric Sciences*, *34*(7), 1149–1152. https://doi.org/10.1175/1520-0469(1977)034<1149:TIOPOT>2.0.CO;2

Vallis, G. (2006). *Atmospheric and oceanic fluid dynamics: Fundamentals and large-scale circulation*. Cambridge: Cambridge University Press. Section 3.8. https://doi.org/10.1017/9781107588417

Vogel, R., Nuijens, L., & Stevens, B. (2016). The role of precipitation and spatial organization in the response of trade-wind clouds to warming. *Journal of Advances in Modeling Earth Systems*, *8*, 843–862. https://doi.org/10.1002/2015MS000568

Voigt, A., Pincus, R., Stevens, B., Bony, S., Boucher, O., Bellouin, N., et al. (2017). Fast and slow shifts of the zonal-mean intertropical convergence zone in response to an idealized anthropogenic aerosol. *Journal of Advances in Modeling Earth Systems*, *9*, 870–892. https://doi.org/10.1002/2016MS000902

Wang, C. (2015). Anthropogenic aerosols and the distribution of past large-scale precipitation change. *Geophysical Research Letters*, *42*, 10,876–10,884. https://doi.org/10.1002/2015GL066416

Zängl, G., Reinert, D., Rípodas, P., & Baldauf, M. (2015). The ICON (ICOsahedral Non-hydrostatic) modelling framework of DWD and MPI-M: Description of the non-hydrostatic dynamical core. *Quarterly Journal of the Royal Meteorological Society*, *141*(687), 563–579. https://doi.org/10.1002/qj.2378